Supplementary data

Boosting the performance of MA-free inverted perovskite solar cells via multifunctional amino acids additives

Chenhui Zhang [a], Chunjun Liang [a]*, Hongkang Gong [a], Jing Wang [b], Qi Song [a], Chao Ji [a], Fulin Sun [a], Ting Zhu [a], Xinghai Huang [a], Yuzhu Guo [a], Dan Li [c]*, Fangtian You [a], Zhiqun He [a]*

[a] *Key Laboratory of Luminescence and Optical Information, Ministry of Education, Institute of Optoelectronic Technology, Beijing Jiaotong University, Beijing 100044, P. R. China*

[b] *Institute for Electric Light Sources, School of Information Science and Technology, Fudan University, Shanghai 200433, P. R. China*

[c] *Department of Physics, School of Physical Science and Engineering, Beijing Jiaotong University, Beijing 100044, P. R. China*

* *Corresponding authors: E-mail addresses: chjliang@bjtu.edu.cn (C. Liang), danli@bjtu.edu.cn (D. Li), zhqhe@bjtu.edu.cn (Z. He).*

List of contents

Experimental section

Materials

PbI_2 (99.99%), $HC(NH_2)_2I$ (FAI, 99.5%), CsI (99.5%), were purchased from TCI; (s)-2-amino-3-phenylpropionic acid hydrochloride (2-ACL, 95%), (s)-3-amino-3-phenylpropionic acid hydrochloride (3-ACL, 97%) from Macklin. Poly[bis(4-phenyl)(2,4,6-triMethylphenyl)aMine] (PTAA) from Xi'an Polymer Light Technology; [6,6]-phenyl-C61-butyric acid methyl ester (PCBM) and Fullerene (C60) from Nano-C; 2,2'-(Perfluorocyclohexa-2,5-diene-1,4-diylidene)dimalononitrile (F4TCNQ) from TCI; zirconium acetylacetonate ($Zr(acac)_4$) from Sigma-Aldrich. All solvents, anhydrous dimethyl sulfoxide (DMSO, extra dry), *N*, *N*-dimethylformamide (DMF, extra dry), toluene, chlorobenzene, 1,2-dichlorobenzene and isopropanol (IPA) were purchased from Acros.

Perovskite precursor: a solution (1.4 M) was prepared by dissolving PbI2 (645.5 mg), FAI (204.3 mg), CsI (50 μl (18.2 mg); note the CsI is prepared of 1.4 M in DMSO in advance) in 1 ml mixed solvent (DMF/DMSO = 4/1(v/v)) for a feed-in composition of $Cs_{0.15}FA_{0.85}PbI_3$. It was further stirring at 60 ^oC for 12 hours.

Perovskite precursor with 2-ACL/3-ACL additive: Dissolve 1.5 mg (0.5 mol%) 2-ACL/3-ACL into 1 ml perovskite precursor. The 2-ACL/3-ACL additive was added into the perovskite precursor 1 hour before films fabrication.

Device fabrication

ITO/glass were sequentially cleaned with soap, deionized water, ethanol under ultrasonication. The substrates were treated with UV ozone for 20 mins. Perovskite films and devices were fabricated in a N_2 glove box. Hole-transport PTAA was dissolved in toluene at 10 mg/ml (with 1%(w/w) F4TCNQ) previously, which was spin-coated on ITO/glass substrates at 6000 r.p.m. for 40 s and annealed at 150℃ for 10 mins. For the perovskite film, 60 μl DMF is used to prewet the PTAA surface with 5000 r.p.m. for 30 s, and then a two-step spin-coating procedure with 1000 rpm for 5 s and 4000 r.p.m. for 30 s was used to fabricate the perovskite films. Chlorobenzene (150 μl) was dropped on the spinning substrate at the last 10 s. The film was then annealed at 100°C for 10 mins. For devices with 2-ACL as the passivation layer, 2-ACL was dissolved in isopropanol at 0.8 mg/ml, which was spin-coated on the annealed perovskite layer 4000 r.p.m. for 40 s. Electron-transport PCBM:C60 (1:1, w/w) was dissolved in dichloride benzene and spin-coated on perovskite/PTAA/ITO/glass substrate at 1000 rpm for 50 s. $Zr(acac)_4$ dissolved in isopropanol was spin-coated on top of the electron transport layer at 4000 rpm for 40 s. Finally, Au (100 nm) was deposited on top of $Zr(acac)_4$ as an electrode using thermally evaporating at 1.0×10^{-6} pa. The active areas of the devices were 0.105 cm^2.

Characterizations of materials

X-ray diffraction (XRD) patterns were taken using a diffractometer (Bruker D8 advance). SEM figures were obtained on a Scanning electron microscopy (SEM)

(Hitachi S4800) working at a 15 kV and a distant of ~8 mm with 20k multiplication using a secondary electron mode. The surface morphologies of the films were measured via atomic force microscope (AFM) (Bruker AXS, Bruker Dension Icon). Steady state photoluminescence (PL) spectra were measured using a fluorescence spectrometer (Horiba Nanolog FL3-2iHR). Time-resolved photoluminescence (TRPL) spectra were obtained with ultrafast lifetime spectrofluorometer (Horiba Delta flex). UV-Vis absorption spectra were taken with UV-Vis-NIR scanning spectrometer (Shimadzu UV-3600). Ultraviolet photoemission spectroscopy (UPS) measurement was measured with an angle-resolved photoemission spectrometer (Thermo escalab 250Xi) using a monochromatic Ar I light source ($h\upsilon$ = 21.22 eV) under a sample bias of -5 V. X-ray photoelectron spectroscopy (XPS) was tested via X-ray photoelectron spectrometer (Thermo escalab 250Xi). Infrared spectra were obtained via Fourier transform infrared spectrometer (FT-IR) (Nicolet IS 10). ^{1}H nuclear magnetic resonance spectra (^{1}H NMR) were measured on a NMR spectrometer (Bruker AVANCE III 600M). Decomposition temperature was tested using via a thermogravimetric analyzer (TGA) (TA instruments, Q600). Impedance of the materials was evaluated using an AC impedance analyzer (Solartron 1260) in frequency range from 1MHz to 0.1Hz at a voltage bias of 0.9V in the dark.

Device testing

Current-voltage (*J-V*) measurements of the devices were tested using a source meter (Keithley 2635B) under illumination of solar simulator (Abet Sun 2000) at a standard

irradiation of AM 1.5G (100 mW/cm^2), the scan rate is 10 mV/s. The external quantum efficiencies (EQE) of the solar cells were detected with a solar cell quantum-efficiency measurement system (Zolix Solar Cell Scan 100).

Conditions for operational stability tests are as follows:

In stability test, *J–V* characteristics were recorded automatically at half an hour interval using a source meter (Keithley 2635B) under illumination of white LED unit at a standard irradiation of AM 1.5G (100 mW/cm^2) in a nitrogen filled glove box at room temperature. In operational stability test, a constant biased voltage (0.9 V) at the maximum power point (MPP) was also applied.

DFT calculations

We have employed the Vienna ab initio simulation package (VASP) [1,2] to perform all density functional theory (DFT) calculations within the generalized gradient approximation (GGA) using the Perdew-Burke-Ernzerhof (PBE) [3] formulation. We have chosen the projected augmented wave (PAW) potentials [4,5] to describe the ionic cores and take valence electrons into account using a plane wave basis set with a kinetic energy cutoff of 400eV. Partial occupancies of the Kohn−Sham orbitals were allowed using the Gaussian smearing method and a width of 0.05 eV. The electronic energy was considered self-consistent when the energy change was smaller than 10−5eV. A geometry optimization was considered convergent when the force change was smaller than 0.05 eV/Å. Grimme's DFT-D3 methodology [6] was used to describe the

dispersion interactions. The Brillourin zone was sampled with a gamma-centered grid 2 × 2 × 1 through all the computational process. [7] Periodic boundary conditions were used in all directions and a vacuum layer of 15 Å was used in the z-direction to separate the slabs.

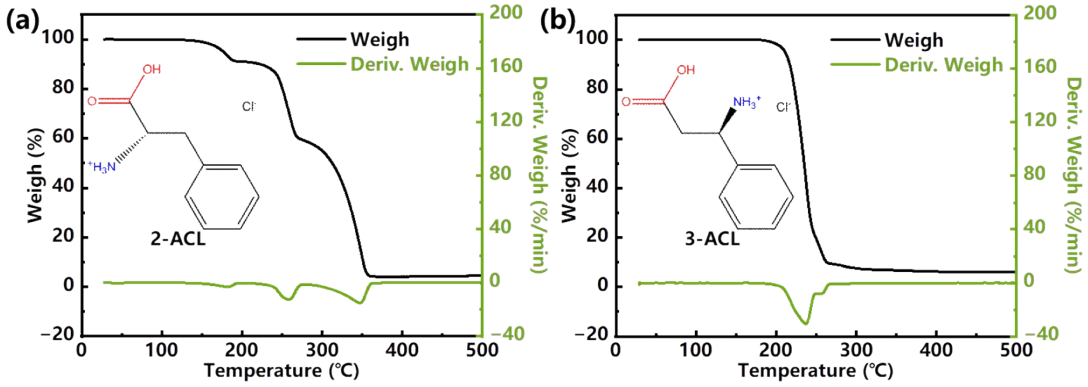

Figure S1. Thermogravimetric analysis spectra of **(a)** 2-ACL and **(b)** 3-ACL.

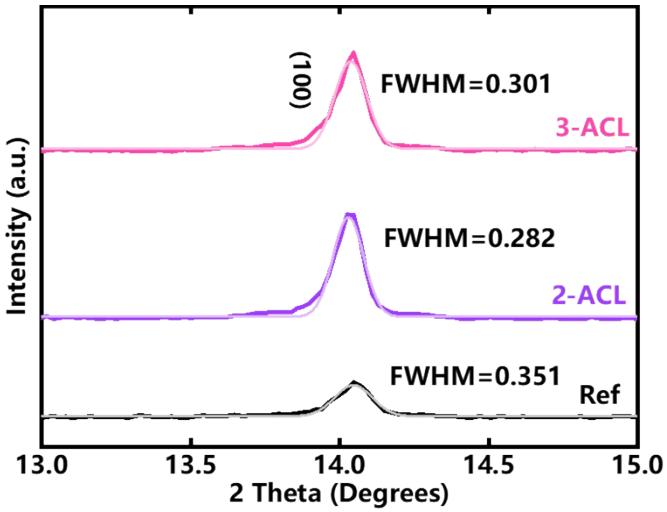

Figure S2. The Gaussian fitting and FWHM values of the (100) peak in XRD testing of different perovskite films

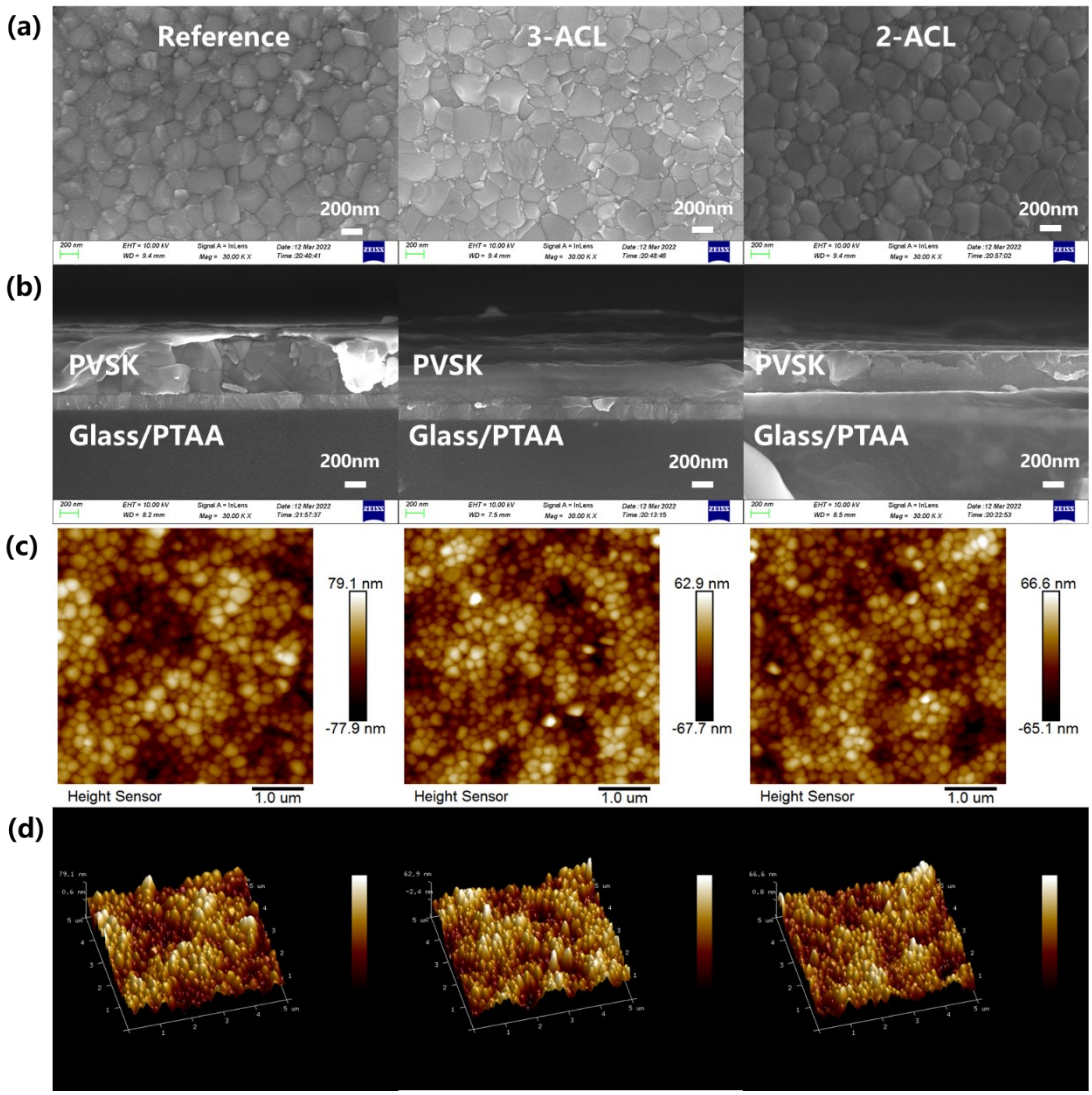

Figure S3. (a) Top-view SEM images **(b)** Cross-sectional SEM images and **(c)** 2D atomic force microscopy (AFM) images **(d)** 3D AFM images of reference, 3-ACL and 2-ACL perovskite films (AFM test area is 5μm × 5μm). The RMS of the reference, 3-ACL and 2-ACL perovskite films is 22.7nm, 19.0nm and 18.5nm, respectively.

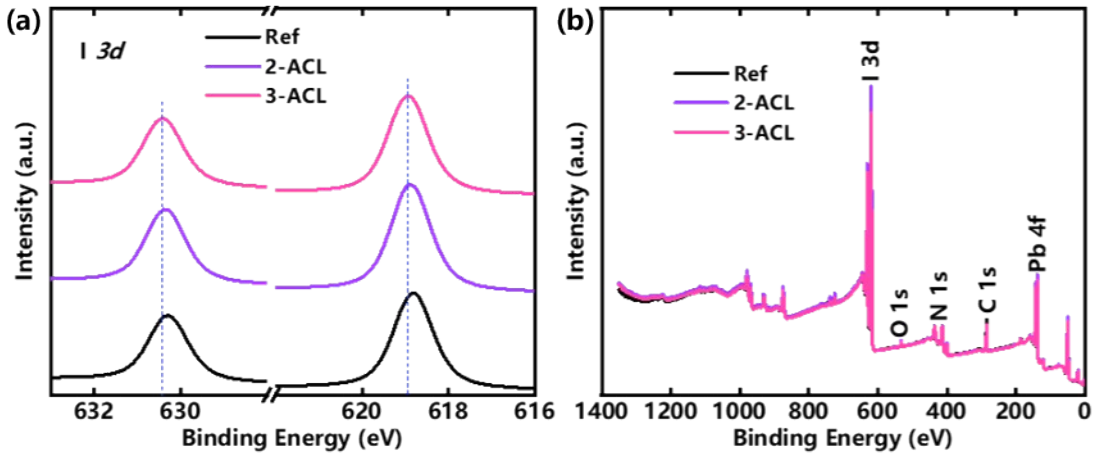

Figure S4. (a) XPS at I 3d orbitals measured from the specimens as indicated. **(b)** XPS spectra of reference, 2-ACL and 3-ACL films.

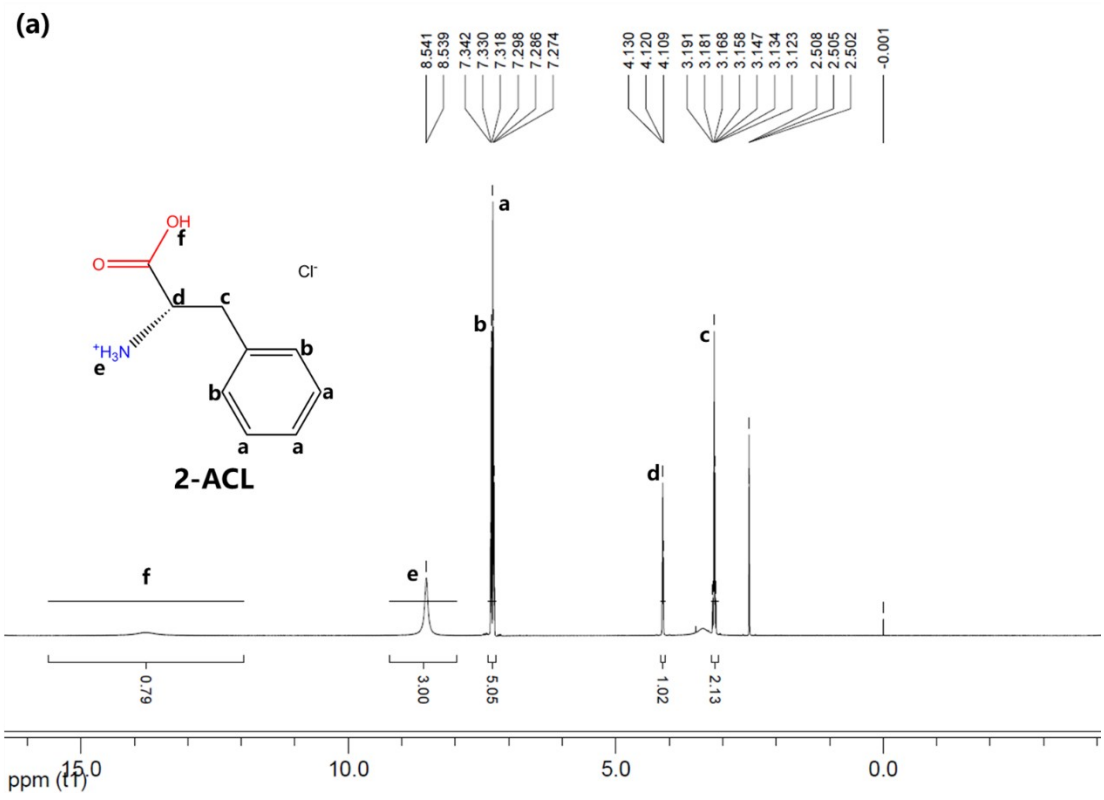

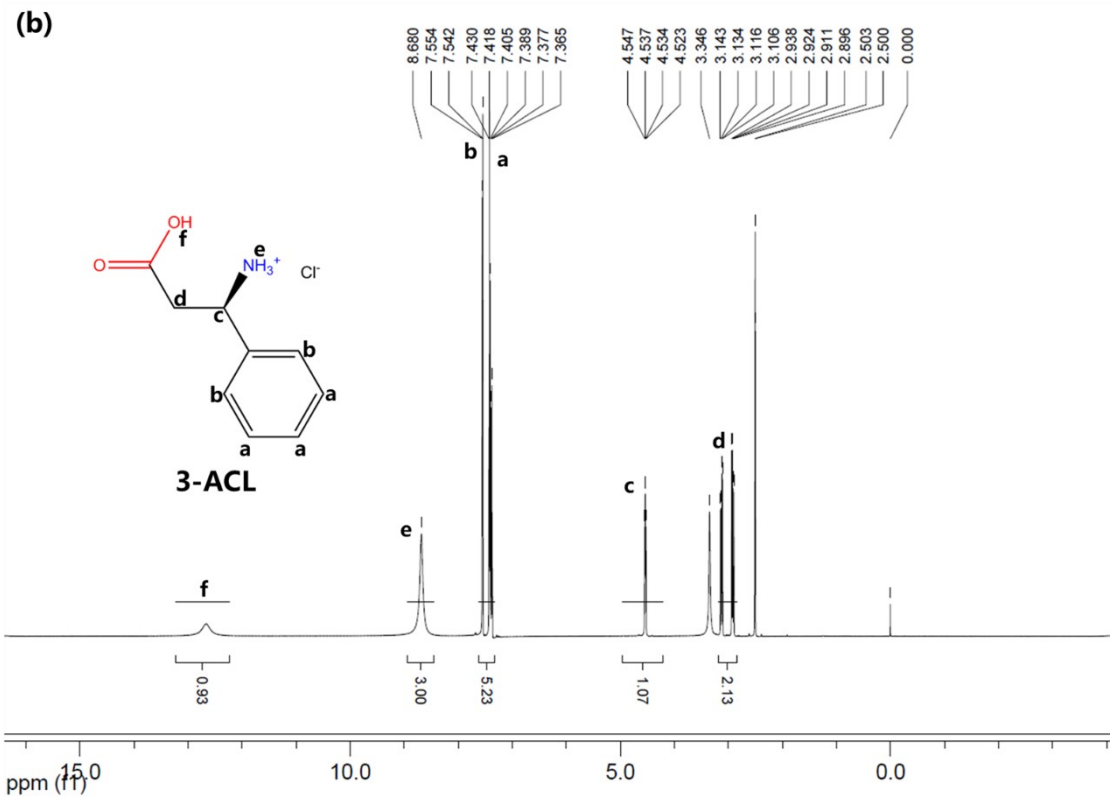
(b)
8.680
7.554
7.542
7.430
7.418
7.405
7.389
7.377
7.365
4.547
4.537
4.534
4.523
3.346
3.143
3.134
3.116
3.106
2.938
2.924
2.911
2.896
2.503
2.500
0.000
OH
O
f
e
NH3+
Cl-
d
c
b
b
a
a
a
3-ACL
f
e
c
d
0.93
3.00
5.23
1.07
2.13
15.0
10.0
5.0
0.0
ppm (f1)

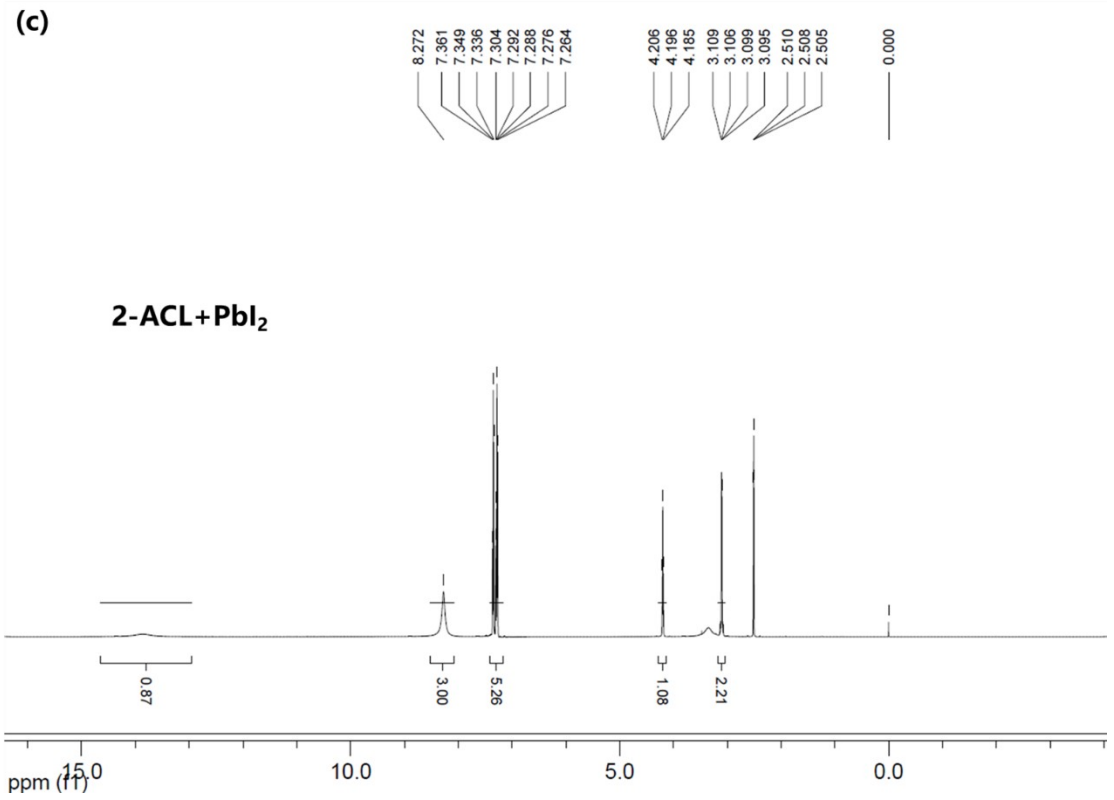
(c)
8.272
7.361
7.349
7.336
7.304
7.292
7.288
7.276
7.264
4.206
4.196
4.185
3.109
3.106
3.099
3.095
2.510
2.508
2.505
0.000
2-ACL+PbI2
0.87
3.00
5.26
1.08
2.21
15.0
10.0
5.0
0.0
ppm (f1)

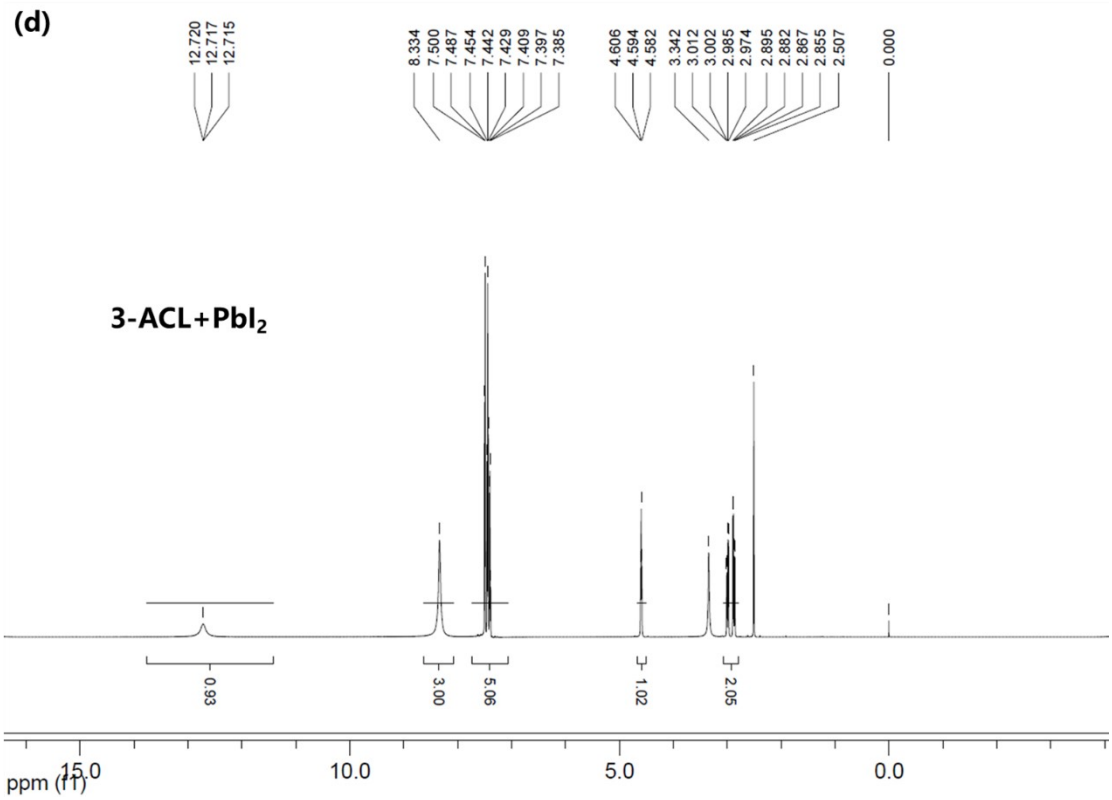

Figure S5. ^{1}H NMR spectra of (a) 2-ACL (b) 3-ACL (c) 2-ACL + PbI_2 and (d) 3-ACL + PbI_2 (d6-DMSO)

Table S1. Detailed fitting parameters of Figure 6a.

Sample	Slpoe	K_BT/q	m
Reference	0.043±0.002	0.02585	1.68±0.07
2-ACL	0.039±0.001	0.02585	1.49±0.04
3-ACL	0.040±0.001	0.02585	1.53±0.05

$V_{oc} = \frac{mk_BT}{q}\ln\left(\frac{J_{SC}}{J_0}\right) = \frac{mk_BT}{q}\ln\left(J_{SC}\right) - \frac{mk_BT}{q}\ln\left(J_0\right) = \frac{mk_BT}{q}\ln\left(J_{SC}\right) + C$, m is the ideal factor, C is a constant [8].

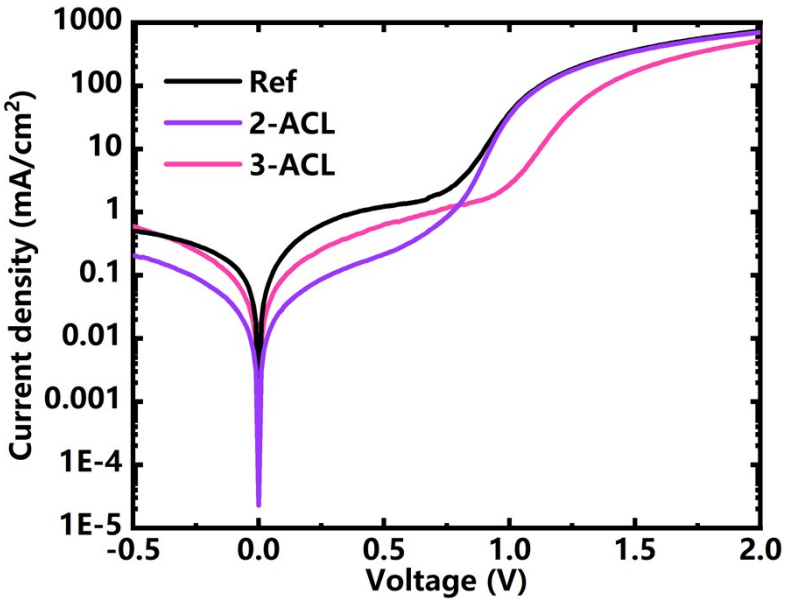

Figure S6. Dark J–V curves of the corresponding devices.

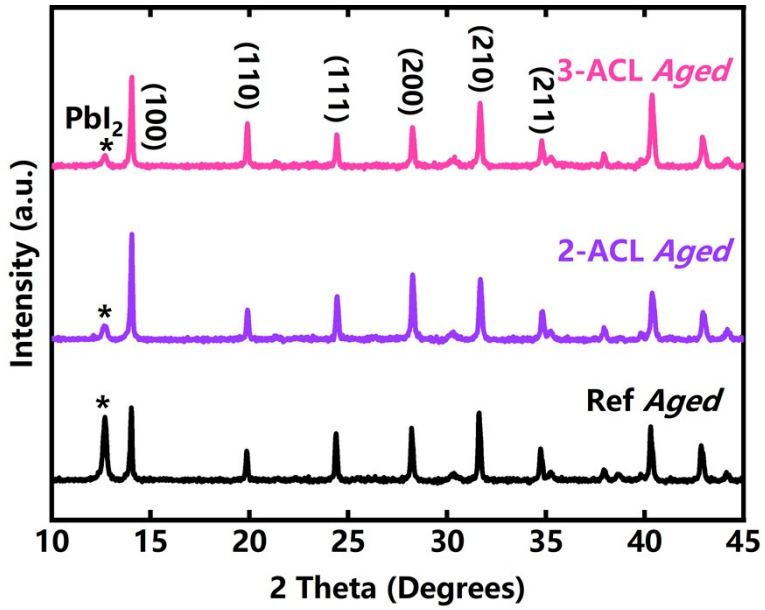

Figure S7. XRD spectra of the aged corresponding films.

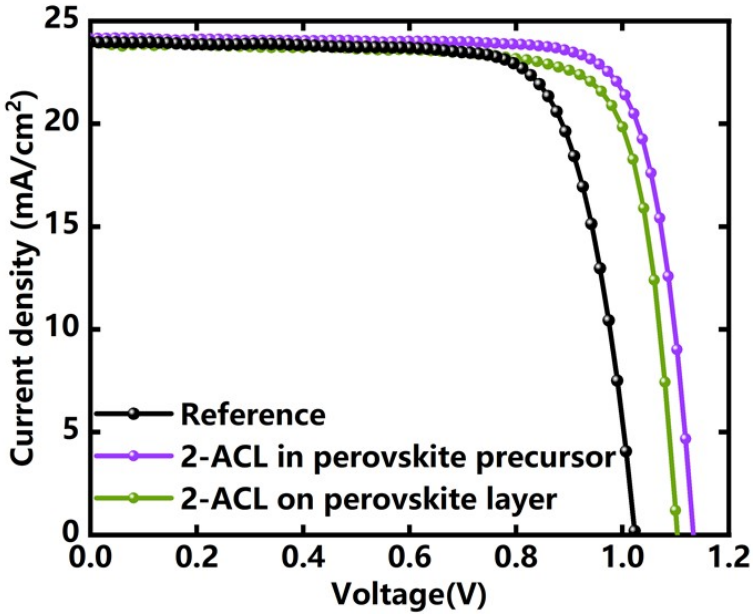

Figure S8. J–V curves of the champion devices with different preparation methods under 1 sun illumination.

Table S2. The parameters of champion devices performance with different preparation methods under 1 sun illumination.

Sample	V_{OC} [V]	J_{SC} [mA/cm^2]	FF [%]	PCE [%]
Reference	1.023	23.98	76.71	18.82
Additive	1.137	24.15	80.16	22.01
Passivation layer	1.101	23.92	78.55	20.69

When amino acids are utilized at the interface, they can only interact with the surface of perovskite, and cannot act on the grain boundaries of perovskite. In contrast, mixing amino acids into the precursor can enable the passivation of both the grain boundary and surface of perovskite, while simultaneously optimizing the crystallization of perovskite, thus resulting in better passivation effects on perovskite.

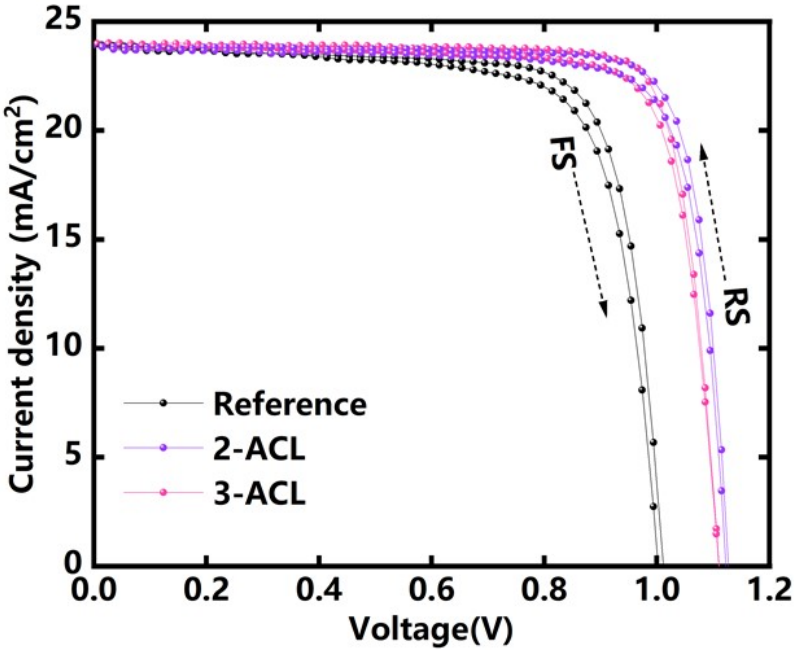

Figure S9. Forward and reverse J–V scans. The testing devices are indicated inside the graphs.

Table S3. Photovoltaic parameters of reverse scan and forward scan for different devices.

Sample	Scan Direction	V_{OC} [V]	J_{SC} [mA/cm^2]	FF [%]	PCE [%]	[a] H-index%
Reference	[b] Reverse	1.012	23.91	76.98	18.62	4.58
	[c] Forward	1.006	23.85	74.16	17.79	
2-ACL	[b] Reverse	1.129	23.82	80.91	21.76	3.26
	[c] Forward	1.122	23.74	79.01	21.05	
3-ACL	[b] Reverse	1.111	23.99	79.69	21.24	2.02
	[c] Forward	1.110	23.80	78.79	20.81	

[a] H-index = (PCE_{RS} - PCE_{FS})/PCE_{RS}. [b] RS: reverse scan, from V_{OC} to 0 V; [c] FS: forward scan, from 0 to V_{OC}.

The results indicate that the hysteresis factor H-index of the PSCs doped with additives was reduced compared to that of the reference device. This finding suggests that the ion migration effect was inhibited to some degree.

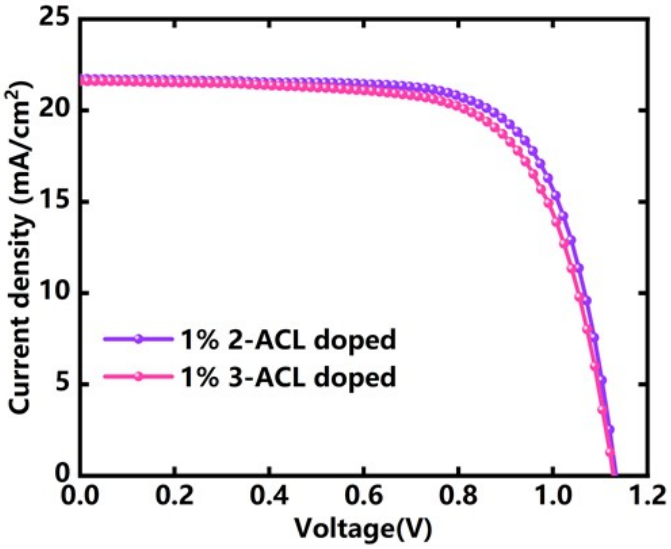

Figure S10. J–V curves of the devices with 1% molar ratio doping concentration of different additives under 1 sun illumination.

Table S4. The parameters of devices performance with 1% molar ratio doping concentration additives of 2-ACL and 3-ACL.

Sample	V_{OC} [V]	J_{SC} [mA/cm^2]	FF [%]	PCE [%]
1% 2-ACL	1.138	21.68	69.79	17.22
1% 3-ACL	1.121	21.59	69.01	16.70

As the doping concentration of additives increases, the presence of additional amino acids contributes to the passivation of perovskite defects, resulting in a slight increase in the V_{OC}. However, their excessive distribution in the perovskite layer may hinder the crystallization and film formation, leading to a decrease in the J_{SC} and FF of

the PSCs. Therefore, increasing the additive concentration beyond the optimal level can lead to a reduction in J_{SC} and FF [9].

Table S5. The fitting PL lifetime of $Cs_{0.15}FA_{0.85}PbI_3$ films with and without optimal molar ratios additive of 2-ACL and 3-ACL. The statistical data were obtained from 10 films for non-doped and each additives-doped.

Sample	A_1	τ_1 (ns)	A_2	τ_2 (ns)	τ_{av}(ns)
Ref	1589.33(44.01%)	11.33	2021.96(55.99%)	274.21	265.94
	1361.79(37.29%)	13.99	2290.11(62.71%)	251.07	243.47
	1354.13(36.61%)	12.34	2344.68(63.39%)	290.45	283.79
	1535.60(41.38%)	14.65	2175.38(58.62%)	249.34	239.99
	1585.39(42.51%)	11.89	2144.07(57.49%)	265.39	257.26
	1588.77(43.87%)	15.25	2032.78(56.13%)	251.04	240.35
	1605.06(39.06%)	14.06	2504.15(60.94%)	246.78	238.58
	1727.78(42.66%)	12.14	2322.33(57.34%)	254.25	245.94
	1478.47(38.25%)	13.07	2386.80(61.75%)	281.29	273.79
	1634.39(43.28%)	12.69	2141.93(56.72%)	263.12	254.23
2-ACL	722.20(17.13%)	16.03	3493.54(82.87%)	1301.54	1298.24
	909.78(21.05%)	16.67	3412.56(78.95%)	1287.28	1282.91
	698.19(16.29%)	19.62	3587.93(83.71%)	1428.21	1424.46
	987.22(22.31%)	18.32	3438.64(77.69%)	1378.76	1373.59
	858.88(19.56%)	20.27	3532.37(80.44%)	1398.32	1393.48

	755.12(17.73%)	19.75	3504.17(82.27%)	1415.08	1410.90
	833.25(18.62%)	19.48	3642.24(81.38%)	1365.17	1360.79
	749.68(16.34%)	17.51	3838.49(83.64%)	1384.49	1381.12
	928.89(20.52%)	19.15	3596.80(79.48%)	1407.57	1402.71
	864.62(19.89%)	18.99	3483.04(81.11%)	1390.66	1386.03
3-ACL	841.77(19.12%)	17.24	3560.80(80.88%)	1160.73	1156.73
	802.55(17.88%)	16.17	3685.97(82.12%)	1217.62	1214.16
	804.19(17.63%)	18.38	3757.27(82.37%)	1059.19	1055.34
	943.21(20.59%)	18.89	3637.70(79.41%)	1129.24	1124.45
	845.72(18.42%)	16.79	3745.57(81.58%)	1087.34	1083.62
	960.64(21.73%)	17.56	3460.14(78.27%)	1257.66	1252.87
	906.25(19.37%)	19.09	3772.39(80.63%)	1134.87	1130.38
	814.98(17.30%)	18.63	3895.87(82.70%)	1181.52	1177.70
	985.42(20.57%)	17.43	3805.13(79.43%)	1197.06	1192.63
	982.48(21.64%)	17.77	3557.63(78.36%)	1231.98	1227.16

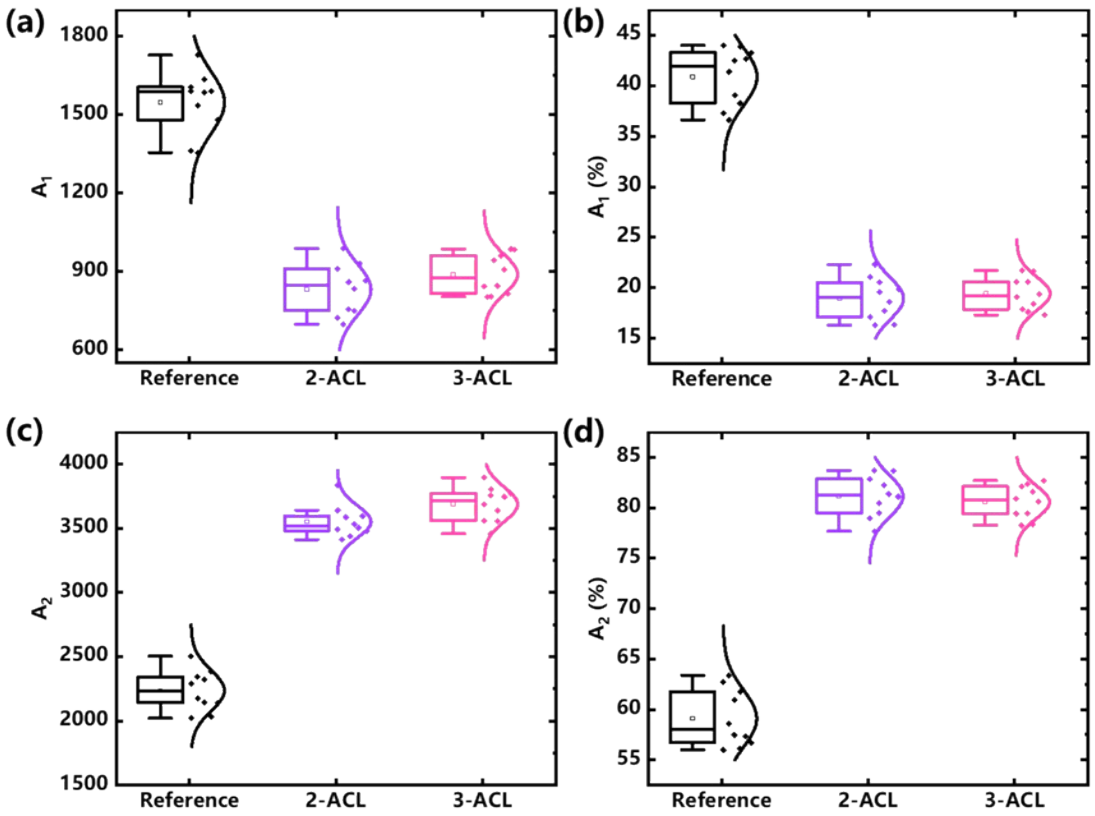

Figure S11. The statistical data of A_1, A_2 from 10 films for non-doped and each additives-doped.

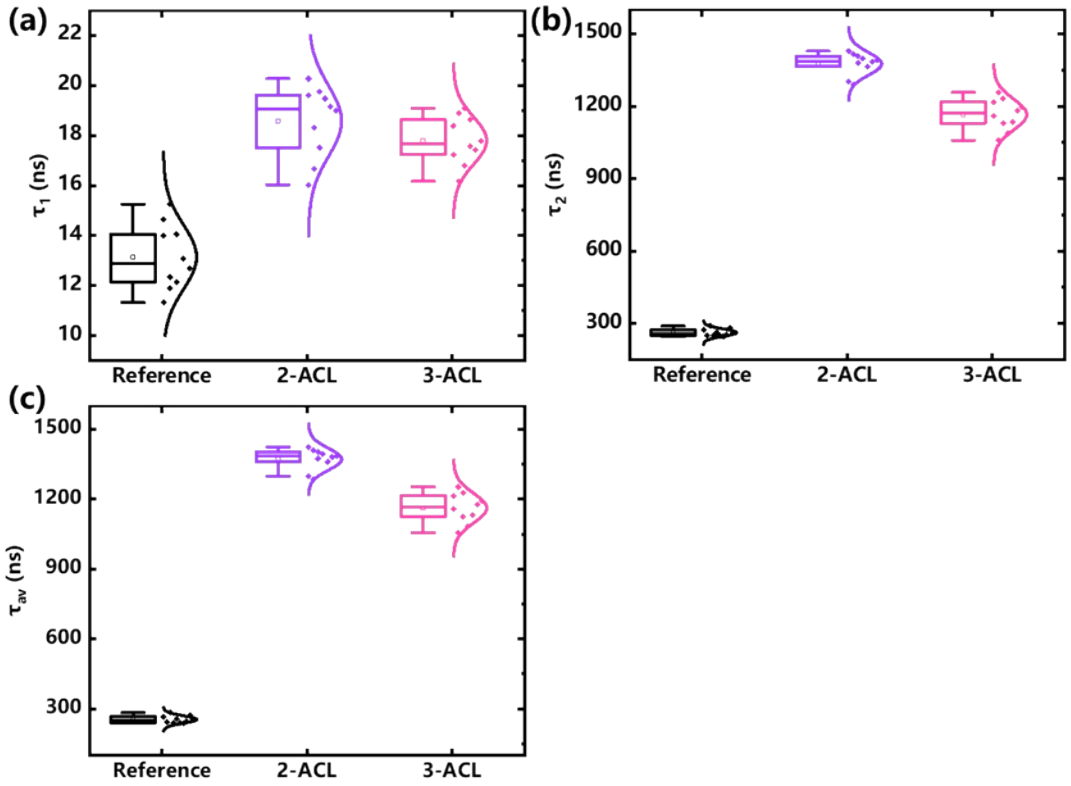

Figure S12. The statistical data of τ_1, τ_2 and τ_{av} from 10 films for non-doped and each additives-doped.

Reference

[1] Kresse, G.; Furthmüller, J. Efficiency of Ab-Initio Total Energy Calculations for Metals and Semiconductors Using a Plane-Wave Basis Set. Comput. Mater. Sci. 199, 6, 15−50.

[2] Kresse, G.; Furthmüller, J. Efficient Iterative Schemes for Ab Initio Total-Energy Calculations Using a Plane-Wave Basis Set. Phys. Rev. B 1996, 54, 11169−11186.

[3] Perdew, J. P.; Burke, K.; Ernzerhof, M. Generalized Gradient Approximation Made Simple. Phys. Rev. Lett. 1996, 77, 3865−3868.

[4] Kresse, G.; Joubert, D. From Ultrasoft Pseudopotentials to the Projector

Augmented-Wave Method. Phys. Rev. B 1999, 59, 1758-1775.

[5] Blöchl, P. E. Projector Augmented-Wave Method. Phys. Rev. B 1994, 50, 17953−17979.

[6] Grimme, S.; Antony, J.; Ehrlich, S.; Krieg, H. J. Chem. Phys. 2010, 132, 154104.

[7] H. J. Monkhorst and J. D. Pack, Phys. Rev. B, 1976, 13, 5188-5192.

[8] Q. Cao, Y. Li, Y. Zhang, J. Zhao, T. Wang, B. Yang, X. Pu, J. Yang, H. Chen, X. Chen, X. Li, S. Ghasemi, H. Salari, A. Hagfeldt and X. Li, Adv Energy Mater, 2022, 12.

[9] P. Xu, L. Xie, S. Yang, B. Han, J. Liu, J. Chen, C. Liu, R. Jia, M. Yang and Z. Ge, Sol Rrl, 2022, 7.